Analysis of Kerr effect in resonator fiber optic gyros with triangular wave phase modulation

D. Ying,* M. S. Demokan, X. Zhang, and W. Jin

Department of Electrical Engineering, The Hong Kong Polytechnic University, Hung Hom, Kowloon, Hong Kong

*Corresponding author: dqying@yahoo.cn

Received 25 August 2009; revised 23 November 2009; accepted 27 November 2009; posted 30 November 2009 (Doc. ID 116139); published 20 January 2010

We present an in-depth analysis of the Kerr effect in resonator fiber optic gyros (R-FOGs) based on triangular wave phase modulation. Formulations that relate gyro output to the rotation rate, the Kerr nonlinearity, and other fiber and gyro parameters are derived and used to study the effect of Kerr nonlinearity on the gyro performance. Numerical investigation shows that the Kerr effect results in a nonzero gyro output even when the gyro is at stationary, which is interpreted as an error in the measurement of rotation rate. This error was found to increase as the frequencies of the two triangular phase modulations deviate from each other, and is not zero even if the intensities of the two counterpropagating beams are exactly the same. For fixed frequencies of the triangular phase modulations, there exists an optimal intensity splitting ratio for the two counterpropagating beams, which leads to zero gyro error. Calculation shows that the measurement error due to the Kerr effect for an R-FOG with a hollow-core photonic bandgap fiber as the fiber loop can be one to two orders of magnitude smaller than an R-FOG with a conventional single mode fiber loop.

OCIS codes: 060.2370, 060.2800.

1. Introduction

Using the Sagnac effect [1], the resonator fiber optic gyro (R-FOG) has been proposed and analyzed [2]. Theoretically an R-FOG has similar shot noise limited performance as an interferometric fiber optic gyro (I-FOG) but requires a shorter length of fiber, and hence would have potentially lower cost [2]. In practice, the performance of R-FOGs lags behind that of the I-FOG, possibly due to the various error sources associated with the use of a highly coherent light source and the resonator configuration, such as Rayleigh backscattering [3,4] and Kerr [5,6], Faraday [7,8], and thermal effects [2,9]. The recent advances in air-core photonic-bandgap fibers (PBFs) could improve the performance of R-FOGs [10,11]. Since the optical mode is mostly propagating in air in the air-core PBFs, the drift due to the aforementioned deleterious effects would be smaller than in a conventional single mode fiber (SMF) in which the optical mode travels in silica [12,13].

Kim, Digonnet, and Kino studied the performance of an I-FOG with an air-core PBF sensing coil and showed that the effects of the deleterious effects can be significantly reduced [13]. And the Kerr effects in the R-FOGs with square-wave frequency modulation [14] and sinusoidal phase modulation [5,15] have been analyzed previously. We here analyze the effect of Kerr nonlinearity on the performance of an R-FOG with triangular phase modulation [16,17] for both the clockwise (CW) and the counterclockwise (CCW) propagating waves, and we evaluate the performance improvement by use of air-core PBF instead of a conventional SMF sensing loop. We focused here our analysis on the triangular phase modulation since it is better in reducing backscatter induced noise as compared to sinusoidal phase modulation [16]. We present a general formulation on the effect of Kerr nonlinearity for an R-FOG based on

0003-6935/10/030529-07$15.00/0

triangular wave phase modulation [16,17], and we provide an expression for the demodulation curve when the Kerr effect is considered. Numerical simulations are then carried out for R-FOGs with air-core PBF and conventional SMF respectively as the sensing loops. The effects of the Kerr nonlinearity on the zero bias for various modulation frequencies and intensity splitting ratios are analyzed. The performance of R-FOGs with air-core air-silica PBF and conventional SMF sensing coils are compared.

2. Theoretical Formulation

Figure 1 illustrates the system configuration of the air-core PBF R-FOG based on the triangular wave phase modulation [16,17]. The fiber ring resonator (FRR) can be made entirely from conventional SMF or from air-core PBF spliced to the two arms of a conventional SMF coupler C4. Other components are all made of or pigtailed with conventional SMFs. The length of the fiber ring is L, and the intensity coupling ratios for couplers C1, C2, and C3 are assumed to be 0.5, while the intensity coupling ratio for coupler C4 is k_C. The center frequency and spectral linewidth of the fiber laser are f_0 and δf, respectively.

$$f_{s_{\mathrm{CW}}}(t) = \begin{cases} 2F_{M\_\mathrm{CW}} & \text{for } \left[\frac{p}{F_{M\_\mathrm{CW}}} < t \le \left(p+\frac{1}{2}\right)\frac{1}{F_{M\_\mathrm{CW}}}\right] \\ -2F_{M\_\mathrm{CW}} & \text{for } \left[\left(p+\frac{1}{2}\right)\frac{1}{F_{M\_\mathrm{CW}}} < t \le (p+1)\frac{1}{F_{M\_\mathrm{CW}}}\right] \end{cases}, \tag{1}$$

where p is an integer. Obviously $f_{s\mathrm{CW}}(t)$ is a periodic function of time with a zero mean. The output electric field of the fiber laser can be written as [5,21]

$$E_{\mathrm{Laser}}(t) = E_0 \exp\{i[2\pi f_0 t + \varphi(t)]\}, \tag{2}$$

where E_0 is the amplitude of the electric field of the laser light, and the phase fluctuation $\varphi(t)$ represents the important parameter of optical source coherence [5,21,22]. The intensity of the CW beam in the FRR can be written as [5,19,21,23]

$$I_{\mathrm{FRR_{CW}}}(t,z) = u_{\mathrm{CW}} \exp(-\alpha_L z) B(f_{\mathrm{CW}} + f_{\mathrm{Kerr}}^{\mathrm{CW}}), \tag{3}$$

where

$$B(X) = I_0 k_C (1-\alpha_C)(1-\alpha_s)\frac{1}{1-(1-k_C)(1-\alpha_C)(1-\alpha_s)^2\exp(-\alpha_L L)} \times \frac{1-(1-k_C)(1-\alpha_C)(1-\alpha_s)^2\exp(-\alpha_L L)\exp(-2\pi\delta f\tau_0)}{1+(1-k_C)(1-\alpha_C)(1-\alpha_s)^2\exp(-\alpha_L L)\exp(-2\pi\delta f\tau_0)-2[(1-k_C)(1-\alpha_C)(1-\alpha_s)^2\exp(-\alpha_L L)]^{1/2}\exp(-\pi\delta f\tau_0)\cos(2\pi X\tau_0)}, \tag{4}$$

The laser with output intensity I_0 is divided into two beams by coupler C1, and each beam is phase modulated by a triangular wave through the use of two $LiNbO_3$ phase modulators PM1 and PM2 before being launched into the FRR. The CW and CCW beams $E_{\mathrm{FRR\_CW}}$ and $E_{\mathrm{FRR\_CCW}}$ in the FRR are sensed in reflection mode by the InGaAs PIN photodetecters PD1 and PD2, respectively. The CW signal is demodulated by the demodulation circuit DMC1, and the demodulated signal is used to lock the center frequency of the fiber laser to the CW resonance of the FRR through the feedback circuit FBC. The CCW signal is demodulated by the demodulation circuit DMC2, and the demodulated signal is proportional to the rotation rate [16,17].

Figure 2 shows the waveform of the triangular wave phase modulation signal φ_{t_CW} for the CW beam, where F_{M_CW} is the modulation frequency, and the phase modulation index is fixed to π rad [16]. This phase modulation is equivalent to a frequency shift [18–20] given by

u_{CW} is the intensity coefficient of the CW beam including the loss at the optical elements such as the phase modulator PM2 [5], α_L is the fiber attenuation in the FRR, $I_0 = {E_0}^2$ is the output intensity of the fiber laser, α_C is the intensity loss of the directional coupler C4, α_s is the fusion-splice loss between PBF and conventional fiber in the FRR, $\tau_0 = n_r L/c$ is the transit time in the FRR, n_r is the effective refractive index of the fundamental mode, c is the light velocity in vacuum, and $f_{\mathrm{Kerr}}^{\mathrm{CW}}$ is the frequency shift due to the Kerr effect [23]. The parameter f_{CW} is defined as

$$f_{\mathrm{CW}} = f_0 - f_{\mathrm{RES}}^{\mathrm{CW}} + f_{s_{\mathrm{CW}}}(t), \tag{5}$$

where $f_{\mathrm{RES}}^{\mathrm{CW}}$ is the CW resonance frequency of the FRR. When the frequency of the CW beam equals to $f_{\mathrm{RES}}^{\mathrm{CW}}$, the resonance of CW propagation occurs in the FRR and the CW output intensity from the FRR becomes minimum. For the open-loop configuration shown in Fig. 1, since the operating point for the

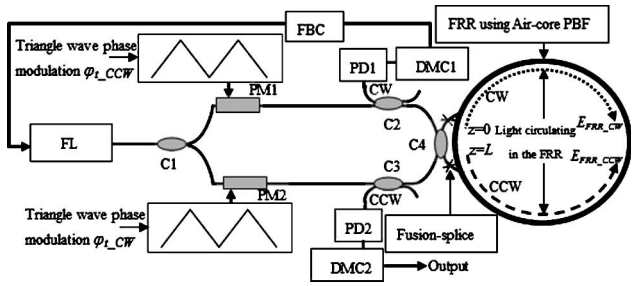

Fig. 1. System configuration of the R-FOG based on the triangular wave phase modulation: FL, fiber laser; CW, clockwise; CCW, counterclockwise; C1–C4, couplers; PD1, PD2, photodetectors; DMC1, DMC2, demodulation circuits; PM1, PM2, phase modulators; FBC, feedback circuit.

CW beam is always fixed at the resonance of the FRR [16,17], $f_{\mathrm{RES}}^{\mathrm{CW}}$ is also the operating frequency of the CW beam. Similarly, the intensity of the CCW beam in the FRR can be derived as [5,19,21,23]

$$I_{\mathrm{FRR_{CCW}}}(t,z) = u_{\mathrm{CCW}} \exp[-\alpha_L(L-z)]B(f_{\mathrm{CCW}} + f_{\mathrm{Kerr}}^{\mathrm{CCW}}), \tag{6}$$

where u_{CCW} is the intensity coefficient of the CCW beam including the loss at the optical elements such as the phase modulator PM1 [5], and $f_{\mathrm{Kerr}}^{\mathrm{CCW}}$ is the frequency shift due to the Kerr effect [23]. The parameter f_{CCW} is defined as

$$\begin{aligned} f_{\mathrm{CCW}} &= f_0 - f_{\mathrm{RES}}^{\mathrm{CCW}} + f_{s_{\mathrm{CCW}}}(t) \\ &= f_0 - f_{\mathrm{RES}}^{\mathrm{CW}} - \Delta f_{\mathrm{RES}} + f_{s_{\mathrm{CCW}}}(t), \end{aligned} \tag{7}$$

where $f_{\mathrm{RES}}^{\mathrm{CCW}}$ is the CCW resonance frequency of the FRR. When the frequency of the CCW beam is $f_{\mathrm{RES}}^{\mathrm{CCW}}$, the resonance of CCW propagation occurs in the FRR, and the CCW output intensity from the FRR reaches a minimum; $f_{s\mathrm{CCW}}(t)$ is the frequency shift resulting from the triangular phase modulation of the CCW beam with the modulation frequency F_{M_CCW} [18–20], which has a similar expression to $f_{s\mathrm{CW}}(t)$ as given in Eq. (1). Δf_{RES} is the difference of the resonance frequencies between the CW and CCW propagating beams and can be written as

$$\Delta f_{\mathrm{RES}} = f_{\mathrm{RES}}^{\mathrm{CCW}} - f_{\mathrm{RES}}^{\mathrm{CW}}. \tag{8}$$

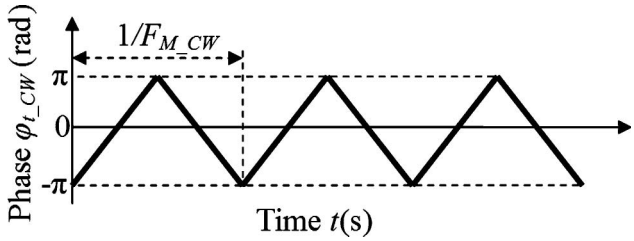

Fig. 2. Waveform of the triangular wave phase modulation signal for CW beam.

The operating point for the CW beam is always fixed at the resonance; therefore, f_0 and $f_{\mathrm{Kerr}}^{\mathrm{CW}}$ satisfy [5,15,23]

$$f_0 + f_{\mathrm{Kerr}}^{\mathrm{CW}} = f_{\mathrm{RES}}^{\mathrm{CW}}. \tag{9}$$

According to Eqs. (3), (5), and (9), we can obtain the intensity of the CW beam in the FRR at the resonance as

$$I_{\mathrm{FRR_{CW}0}}(t,z) = u_{\mathrm{CW}} \exp(-\alpha_L z)B(f_{s_{\mathrm{CW}}}). \tag{10}$$

However, the operating point for the CCW beam is not always fixed at the resonance for the configuration shown in Fig. 1 [17]. According to Eqs. (6), (7), and (9), we can obtain the intensity of the CCW beam in the FRR when the CW beam is fixed at the resonance as

$$\begin{aligned} I_{\mathrm{FRR_{CCW}0}}(t,z) &= u_{\mathrm{CCW}} \exp[-\alpha_L(L-z)] \\ &\quad \times B(f_{\mathrm{Kerr}}^{\mathrm{CCW}} - f_{\mathrm{Kerr}}^{\mathrm{CW}} - \Delta f_{\mathrm{RES}} + f_{s_{\mathrm{CCW}}}). \end{aligned} \tag{11}$$

According to Eqs. (10) and (11), the frequency shifts due to the Kerr effect can be derived as [5,15,23]

$$\begin{aligned} f_{\mathrm{Kerr}}^{\mathrm{CW}} &= \frac{1}{2\pi\tau_0}\int_0^L \Delta\beta_{K_{\mathrm{CW}}0}\mathrm{d}z = \frac{1}{2\pi\tau_0}\frac{2\omega Z n_2}{cA} \\ &\quad \times \frac{1-\exp(-\alpha_L L)}{\alpha_L}[u_{\mathrm{CW}}B(f_{s_{\mathrm{CW}}}) \\ &\quad + 2u_{\mathrm{CCW}}B(f_{\mathrm{Kerr}}^{\mathrm{CCW}} - f_{\mathrm{Kerr}}^{\mathrm{CW}} - \Delta f_{\mathrm{RES}} + f_{s_{\mathrm{CCW}}})], \end{aligned} \tag{12a}$$

$$\begin{aligned} f_{\mathrm{Kerr}}^{\mathrm{CCW}} &= \frac{1}{2\pi\tau_0}\int_0^L \Delta\beta_{K_{\mathrm{CCW}}0}\mathrm{d}z = \frac{1}{2\pi\tau_0}\frac{2\omega Z n_2}{cA} \\ &\quad \times \frac{1-\exp(-\alpha_L L)}{\alpha_L}[u_{\mathrm{CCW}}B(f_{\mathrm{Kerr}}^{\mathrm{CCW}} - f_{\mathrm{Kerr}}^{\mathrm{CW}} - \Delta f_{\mathrm{RES}} \\ &\quad + f_{s_{\mathrm{CCW}}}) + 2u_{\mathrm{CW}}B(f_{s_{\mathrm{CW}}})], \end{aligned} \tag{12b}$$

where $\Delta\beta_{K_{\mathrm{CW}}0}$ and $\Delta\beta_{K_{\mathrm{CCW}}0}$ are the perturbation of the propagation constant induced by the Kerr effect in CW and CCW beams [5,15,23], ω is the center angular frequency of the laser, Z is the impedance of the fiber, A is the mode filled area, and n_2 is the Kerr coefficient. Subtracting Eq. (12a) from Eq. (12b), we can obtain

$$\begin{aligned} \Delta f_{\mathrm{Kerr}} &= \frac{1}{2\pi\tau_0}\frac{2\omega Z n_2}{cA}\frac{1-\exp(-\alpha_L L)}{\alpha_L}[u_{\mathrm{CW}}B(f_{s_{\mathrm{CW}}}) \\ &\quad - u_{\mathrm{CCW}}B(\Delta f_{\mathrm{Kerr}} - \Delta f_{\mathrm{RES}} + f_{s_{\mathrm{CCW}}})], \end{aligned} \tag{13a}$$

where Δf_{Kerr} is given by

$$\Delta f_{\mathrm{Kerr}} = f_{\mathrm{Kerr}}^{\mathrm{CCW}} - f_{\mathrm{Kerr}}^{\mathrm{CW}}. \tag{13b}$$

According to Eq. (1), both $f_{s_{CW}}$ and $f_{s_{CCW}}$ are periodic functions of time t; therefore, the solution Δf_{Kerr} of Eq. (13a) is also a periodic function of time, and the period of Δf_{Kerr} is decided by the periods of $f_{s_{CW}}$ and $f_{s_{CCW}}$. However, $B(f_{s_{CW}})$ is a constant in Eq. (13a) because $B(2F_{M\_CW})$ equals $B(-2F_{M\_CW})$, and the value of Δf_{Kerr} changes only when $f_{s_{CCW}}$ changes between the two frequency shifts $2F_{M\_CCW}$ and $-2F_{M\_CCW}$; therefore, the period of Δf_{Kerr} is $1/F_{M\_CCW}$. The output signal of the photodetector PD2 can be written as [16,21,24]

$$I_{D_{CCW}}(\Delta f_{RES}) = \frac{1}{2}N(1-\alpha_{C3})(1-\alpha_C) \times \left[1-\rho\frac{(1-Q)^2}{(1-Q)^2+4Q\sin^2(\pi\cdot F_{CCW}\tau_0)}\right] \times u_{CCW}I_0, \quad (14a)$$

where α_{C3} is the intensity loss of the coupler C3, and N is the photoelectric conversion coefficient of the photodetector PD2. F_{CCW} is defined as $F_{CCW} = f_{CCW} + f_{Kerr}^{CCW}$; according to Eqs. (7), (9), and (13b), it can be written as

$$F_{CCW} = f_0 - f_{RES}^{CW} - \Delta f_{RES} + f_{s_{CCW}}(t) + f_{Kerr}^{CCW} = \Delta f_{Kerr}(t) - \Delta f_{RES} + f_{s_{CCW}}(t), \quad (14b)$$

and other parameters can be written as [16,21,24]

$$\rho = 1 - \frac{1}{1-\alpha_C}\cdot\left[T^2 - \frac{2TR}{1-Q} + \frac{(R')^2}{1-(Q')^2}\cdot\frac{1+Q}{1-Q}\right], \quad (14c)$$

$$T = \sqrt{1-k_C}\cdot\sqrt{1-\alpha_C}, \quad (14d)$$

$$R' = k_C\cdot(1-\alpha_C)\cdot\exp(-\alpha_L L/2)\cdot(1-\alpha_s), \quad R = R'\exp(-\pi\delta f\tau_0), \quad (14e)$$

$$Q' = \exp(-\alpha_L L/2)\cdot(1-\alpha_s)\cdot\sqrt{1-k_C}\cdot\sqrt{1-\alpha_C}, \quad Q = Q'\exp(-\pi\delta f\tau_0). \quad (14f)$$

Here, both $\Delta f_{Kerr}(t)$ and $f_{s_{CCW}}(t)$ in Eq. (14b) are period functions of time; therefore, $I_{D_{CCW}}$ is a periodic function of time also, and the period is $1/F_{M\_CCW}$. The demodulation signal in this R-FOG system is obtained by the cross correlation of $I_{D_{CCW}}$, and the synchronizing square signal $S_{CCW}(t)$, and $S_{CCW}(t)$ can be written as [16]

$$S_{CCW}(t) = \begin{cases} 1 & \text{for } \left[\frac{q}{F_{M\_CCW}} < t \le \left(q+\frac{1}{2}\right)\frac{1}{F_{M\_CCW}}\right] \\ -1 & \text{for } \left[\left(q+\frac{1}{2}\right)\frac{1}{F_{M\_CCW}} < t \le (q+1)\frac{1}{F_{M\_CCW}}\right] \end{cases}, \quad (15)$$

where q is an integer. Using the output signal I_{DCCW}, i.e., Eq. (14a), and the synchronizing square signal S_{CCW}, i.e., Eq. (15), the demodulation signal can be written as [16]

$$V_d = GF_{M\_CCW}\int_0^{1/F_{M\_CCW}} I_{D_{CCW}}(\Delta f_{RES})S_{CCW}(t)dt, \quad (16)$$

where G is the gain of the demodulation circuit DMC2. According to Eq. (14a), because $I_{D_{CCW}}$ is a function of Δf_{RES}, the demodulation signal V_d is also a function of Δf_{RES}.

3. Simulation and Discussion

Based on Eqs. (14)–(16), we carried out numerical simulation on the performance of R-FOGs with an air-core PBF and a conventional SMF sensing loop. Figure 3 shows the calculated demodulation curve near $\Delta f_{RES} = 0$ of the R-FOG for an air-core PBF sensing loop. The modulation frequency of the CW beam is fixed to $F_{M\_CW} = 62.5$ kHz [17,18], while the modulation frequency for the CCW beam takes three different values of $F_{M\_CCW} = 62.5$ kHz, 60 kHz, and 70 kHz. The output intensity I_0 of the fiber laser is assumed to be 1 mW, and the center frequency and the spectral linewidth of the laser are $f_0 \approx 1.9\times10^{14}$ Hz and $\delta f = 60$ kHz, respectively [16]; the fiber length L of the FRR is 20 m [19], the effective refractive index n_r of the PBF is 0.99, the mode filled area A is 4.42×10^{-11} m^2, and the impedance Z is 380.53 [15]; the Kerr coefficient can be expressed as [13]

$$n_2 = \eta n_{2,silica} + (1-\eta)n_{2,air}, \quad (17)$$

where η is the fractional amount of fundamental mode power confined to the solid portions of the PBF, and $n_{2,silica}$ and $n_{2,air}$ are, respectively, the Kerr coefficients of silica and air and take the values of 2.32×10^{-20} m^2/W and 2.9×10^{-23} m^2/W; $\eta = 0.015$ [15]. The intensity coupling ratio k_C is 5%, the

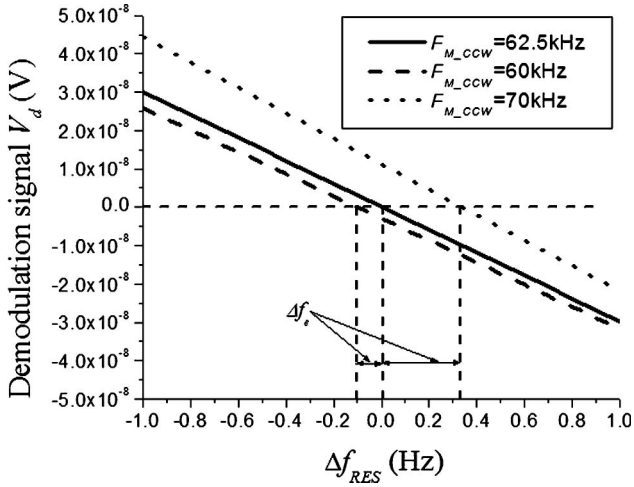

Fig. 3. PBF R-FOG's demodulation curve with different modulation frequencies for CCW beam.

coupler intensity loss α_C is 6.67%, the loss α_{C3} for the coupler C3 is 6.67% [16], the fiber attenuation α_L is 20 dB/km, the splice loss between PBF and conventional SMF α_s is 20.57% (1 dB) [15], the total gain G of the demodulation circuit DMC2 is 1, and the photoelectric conversion coefficient N is 6.25 V/mW [16]. The intensity coefficients of the two counterpropagating beams u_{CW} and u_{CCW} are assumed to be the same and equal to 0.12. As shown in Fig. 3, for $F_{M\_\mathrm{CCW}} = 62.5$ kHz, the demodulation output V_d equals to zero for $\Delta f_{\mathrm{RES}} = 0$, indicating no error occurs under the condition that $u_{\mathrm{CW}} = u_{\mathrm{CCW}}$ and $F_{M\_\mathrm{CW}} = F_{M\_\mathrm{CCW}}$. However, when F_{M_CCW} deviates from F_{M_CW}, the value of Δf_{RES} at the zero-crossing point would not be zero but equals to "Δf_e" as indicated in Fig. 3. This will induce an error "Ω_e" in the measurement of rotation rate.

For a particular value of "F_{M_CCW}", Δf_e can be obtained by solving

$$V_d(\Delta f_{\mathrm{RES}})|_{\Delta f_{\mathrm{RES}}=\Delta f_e} = 0. \tag{18}$$

Once "Δf_e" is obtained, the measurement error in terms of rotation rate may be obtained by using the well known relationship between the frequency difference of the counterpropagating waves and the rotation rate (i.e., the Sagnac effect) and expressed as [25,26]

$$\Omega_e = \frac{\Delta f_e \cdot n_r \cdot \lambda}{D}, \tag{19}$$

where λ is the wavelength of the laser, and D is the diameter of the FRR.

Figure 4 shows the calculated measurement error (Ω_e) due to the Kerr effect as a function of modulation frequency $F_{M_{\mathrm{CCW}}}$ for $u_{\mathrm{CW}} = u_{\mathrm{CCW}} = 0.12$. The wavelength λ of the laser is 1550 nm, and the diameter D of the FRR is 10 cm [18]. Other parameters have been shown previously in the first paragraph of Section 3. Figure 4(a) is the result of the PBF R-FOG, and Fig. 4(c) shows the same result for a conventional fiber R-FOG. The parameters for the conventional fiber are as follows: $n_r = 1.45$, $A = 5.54 \times 10^{-11}\,\mathrm{m}^2$, $Z = 259.81$, and $\alpha_L = 0.2$ dB/km [15]. Since all the fiber and component parameters are from commercial data sheets, the results shown in Fig. 4(a) would represent the gyro performance achievement with the current technology. However, under this practical condition, the shot noise limited sensitivity [1,2,21] for the PBF R-FOG is about 2.19°/h with the photodetector quantum efficiency $\eta = 0.8$ and integration time $t_0 = 1$ s [5], and it is more than an order of magnitude larger than that for the conventional fiber R-FOG, which is about 0.12°/h. To probe further the potential of the air-core fiber technology, we calculated Ω_e as a function of F_{M_CCW} for $\alpha_L = 5$ dB/km and a reduced splice loss of 0.2 dB between the sensing PBF and SMF coupler. Such a small loss is not achievable currently; however, it could be achieved in the future by, for example, fabricating directional coupler directly on air-core PBFs. The result is shown in Fig. 4(b). Under this "ideal" condition, the shot noise limited sensitivity for the PBF R-FOG would be improved to about 0.36°/h, which is the same order of magnitude as that for the conventional fiber R-FOG. It is shown in Fig. 4 that the error Ω_e is zero when F_{M_CCW} equals F_{M_CW}. The error increases as F_{M_CCW} deviates more from F_{M_CW}. Therefore, keeping F_{M_CCW} and F_{M_CW} to be the same is advantageous in reducing the zero point error due to the Kerr effect. However, in the practical R-FOG system, the differences of the frequency shifts $f_{s_{\mathrm{CW}}}$ and $f_{s_{\mathrm{CCW}}}$ are generally chosen to be larger than the gyro signal bandwidth Δf_{bw} for the purpose of elimination of the Rayleigh backscattering [4,5,19,20], which means the difference of the

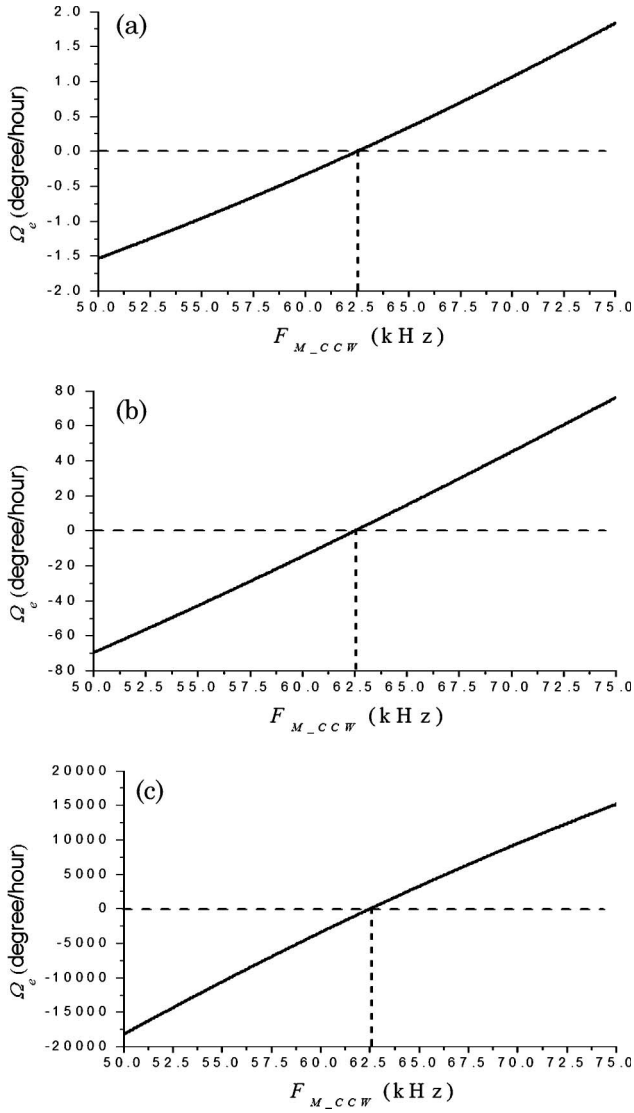

Fig. 4. Relationship between the Kerr-induced error Ω_e and modulation frequency F_{M_CCW} when the intensity coefficients of the two counterpropagating beams u_{CW} and u_{CCW} are the same: (a) result of the PBF R-FOG with practical parameters, (b) result of the PBF R-FOG with "ideal" parameters, and (c) result of the conventional fiber R-FOG.

modulation frequencies F_{M_CW} and F_{M_CCW} should be larger than $\Delta f_{bw}/2$ according to Eq. (1); therefore, the error always exists even if $u_{CW} = u_{CCW}$. From Figs. 4(a) and 4(b) with 4(c), it can be concluded that the Kerr-induced error is much smaller for the PBF R-FOG than for conventional SMF based R-FOG. Taking the gyro with $\Delta f_b = 100$ Hz as an example [18], the modulation frequency F_{M_CCW} could be chosen to be larger than 62.55 kHz; therefore, Ω_e is larger than approximately 0.32°/h for the PBF R-FOG with "ideal" parameters and 92.72°/h for the conventional fiber R-FOG. The significant reduction in the Kerr-related measurement error is because of the much smaller Kerr coefficient of the PBF [13,15].

From the results of Figs. 3 and 4, it is clear that the Kerr-induced error Ω_e would not be completely removed even when $u_{CCW} = u_{CW}$. To see the effect of unequal intensity coefficients u_{CW} and u_{CCW}, we plot in Fig. 5 the relationship between Ω_e and $\Delta u = u_{CCW} - u_{CW}$ for $F_{M\_CCW} = 62.5$ kHz, $F_{M\_CCW} = 60$ kHz, and $F_{M\_CCW} = 70$ kHz, while F_{M_CW} is fixed to 62.5 kHz [17,18]. Figure 5(a) is the result for PBF R-FOG with "ideal" parameters, and Fig. 5(b) is the result for the conventional fiber R-FOG. The intensity coefficient of the CW beam u_{CW} is fixed to 0.12, and other parameters are the same as mentioned in the first and third paragraphs of Section 3. As shown in Fig. 5, for a specific F_{M_CCW} there exists an optimum value of Δu that leads to $\Omega_e = 0$. The value of Δu is larger if F_{M_CCW} is deviated more from F_{M_CW}. Therefore, when we design the R-FOG system, keeping the intensity coefficient to be the same is not conducive to reducing the error caused by the Kerr effect, and we should choose the optimum Δu according to the modulation frequencies. It is also clear that when Δu deviates from its optimum value, the error Ω_e is significantly smaller for the PBF R-FOG than for conventional SMF R-FOG. For example, when F_{M_CCW} is 60 kHz, the optimum Δu is about −0.0012 for the PBF R-FOG and −0.0045 for the conventional fiber R-FOG, and when the Δu deviates from its optimum value for about 0.001, the errors are about −10.76°/h for the PBF R-FOG and −741.73°/h for the conventional fiber R-FOG.

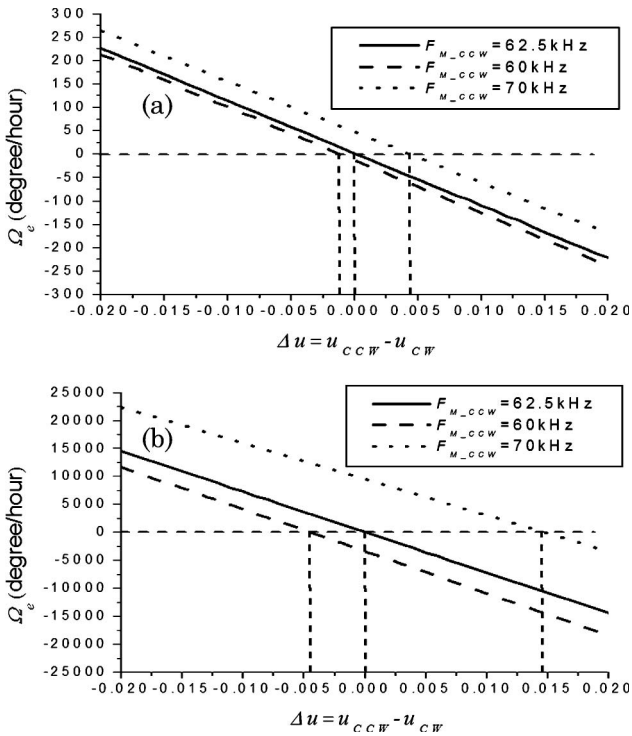

Fig. 5. Relationship between the zero point error Ω_e and difference of the intensity coefficients Δu with different modulation frequencies for CCW beam: (a) result of the PBF R-FOG with "ideal" parameters and (b) result of the conventional fiber R-FOG.

4. Conclusions

The Kerr effect in an air-core PBF R-FOG based on triangular wave phase modulation has been analyzed. It is concluded that when the modulation frequencies for the two counterpropagating beams are different, measurement error due to the Kerr effect would occur even if the intensity coefficients of the two counterpropagating beams are the same. The error increases as the two modulation frequencies deviate more from each other. It is also found that there exists an optimum difference of the intensity coefficients that leads to zero gyro error; this difference would not be zero when the two modulation frequencies are different, and it varies as the difference of the two modulation frequencies varies. The Kerr-induced error in a PBF R-FOG is found to be one to two orders of magnitude smaller than that in a conventional fiber R-FOG. With air-core PBF as the sensing loop, it's possible to achieve Kerr-induced error of smaller than 10.76°/h if Δu is controlled to be better than 0.001. This error could be further reduced by using square wave intensity modulation as described in [5]. Apart from the Kerr effect, the air-core PBF is also better than conventional fiber in reducing the errors due to thermal and Faraday effects. Hence, it is expected that using air-core PBF instead of conventional fiber has the potential to improve the performance of the R-FOG significantly.

The research was partly supported by the Hong Kong SAR government through a Competitive Earmarked Research Grant (CERG) (PolyU5187/06E).

References

1. W. W. Chow, J. Gea-Banaciloche, and L. M. Pedrotti, "The ring laser gyro," Rev. Mod. Phys. **57**, 61–103 (1985).
2. D. M. Shupe, "Fiber resonator gyroscope: sensitivity and thermal nonreciprocity," Appl. Opt. **20**, 286–289 (1981).
3. K. Iwatsuki, K. Hotate, and M. Higashiguchi, "Resonance characteristics of backscattering in optical passive-ring resonator gyro: experiment," Appl. Opt. **25**, 4448–4451 (1986).
4. K. Iwatsuki, K. Hotate, and M. Higashiguchi, "Effect of Rayleigh backscattering in an optical passive ring-resonator gyro," Appl. Opt. **23**, 3916–3924 (1984).
5. K. Iwatsuki, K. Hotate, and M. Higashiguchi, "Kerr effect in an optical passive ring-resonator gyro," J. Lightwave Technol. **4**, 645–651 (1986).

6. K. Takiguchi and K. Hotate, "Method to reduce the optical Kerr-effect-induced bias in an optical passive ring-resonator gyro," IEEE Photonics Technol. Lett. **4**, 203–206 (1992).
7. K. Hotate and K. Tabe, "Drift of an optical fiber gyroscope caused by the Faraday effect: experiment," J. Lightwave Technol. **5**, 997–1001 (1987).
8. T. Ito and K. Hotate, "Closed-loop operation in the resonator fiber optic gyro using Faraday effect with a twisted single-mode-fiber resonator," Proc. SPIE **2837**, 260–271 (1996).
9. K. Hotate and Y. Kikuchi, "Analysis of thermo-optically induced bias drift in resonator fiber optic gyro," Proc. SPIE **4204**, 81–88 (2001).
10. R. F. Cregan, B. J. Mangan, J. C. Knight, T. A. Birks, P. St. J. Russell, P. J. Roberts, and D. C. Allan, "Single-mode photonic band gap guidance of light in air," Science **285**, 1537–1539 (1999).
11. G. A. Sanders, L. K. Strandjord, and T. C. Qiu, "Hollow core fiber optic ring resonator for rotation sensing," in *Optical Fiber Sensors* (Optical Society of America, 2006), paper ME6.
12. C. M. Smith, N. Venkataraman, M. T. Gallagher, D. Muller, J. A. West, N. F. Borrelli, D. C. Allan, and K. W. Koch, "Low-loss hollow-core silica/air photonic bandgap fibre," Nature **424**, 657–659 (2003).
13. H. K. Kim, M. J. F. Digonnet, and G. S. Kino, "Air-core photonic-bandgap fiber-optic gyroscope," J. Lightwave Technol. **24**, 3169–3174 (2006).
14. Q. Yao, Y. Hu, Z. Song, and Y. Xie, "Study on Kerr-effect-induced bias reduction method for resonator fiber optic gyroscope," Acta Photonica Sin. **34**, 1320–1323 (2005).
15. X. Yu, Y. Liao, M. Zhang, Y. Yu, and D. Li, "Kerr effect in an optical passive ring-resonator gyro using a hollow-core photonic band-gap fiber," Chin. J. Lasers **35**, 430–435 (2008).
16. D. Ying, H. Ma, and Z. Jin, "Resonator fiber optic gyro using the triangle wave phase modulation technique," Opt. Commun. **281**, 580–586 (2008).
17. Z. Jin, Z. Yang, H. Ma, and D. Ying, "Open-loop experiments in a resonator fiber-optic gyro using digital triangle wave phase modulation," IEEE Photonics Technol. Lett. **19**, 1685–1687 (2007).
18. D. Ying, H. Ma, and Z. Jin, "Dynamic characteristics of R-FOG based on the triangle wave phase modulation technique," Opt. Commun. **281**, 5340–5343 (2008).
19. K. Hotate and M. Harumoto, "Resonator fiber optic gyro using digital serrodyne modulation," J. Lightwave Technol. **15**, 466–473 (1997).
20. K. Hotate and G. Hayashi, "Resonator fiber optic gyro using digital serrodyne modulation-method to reduce the noise induced by the backscattering and closed-loop operation using digital signal processing," Proc. SPIE **3746**, 104–107 (1999).
21. H. Ma, Z. Jin, C. Ding, and Y. Wang, "Influence of spectral linewidth of laser on resonance characteristics in fiber ring resonator," Chin. J. Lasers **30**, 731–734 (2003).
22. Y. Ohtsuka, "Optical coherence effects on a fiber-sensing Fabry-Perot interferometer," Appl. Opt. **21**, 4316–4320 (1982).
23. X. Zhang, H. Ma, C. Ding, and Z. Jin, "Optical Kerr effect in phase modulation spectroscopy resonator fiber optic gyro," Chin. J. Lasers **33**, 814–818 (2006).
24. H. Ma, Z. Jin, C. Ding, and Y. Wang, "Research on signal detection method of resonator fiber optical gyro," Chin. J. Lasers **31**, 1001–1005 (2004).
25. R. E. Meyer, S. Ezekiel, D. W. Stowe, and V. J. Tekippe, "Passive fiber-optic ring resonator for rotation sensing," Opt. Lett. **8**, 644–646 (1983).
26. H. C. Lefevre, *The Fiber-Optic Gyroscope* (Artech, 1993).